Research Article

XRD Peak Profile Analysis of SiC Reinforced Al$_2$O$_3$ Ceramic Composite Synthesized by Electrical Resistance Heating and Microwave Sintering: A Comparison

Madhan Mohankumar [iD],[1] **S. Praveen Kumar**,[2] **B. Guruprasad** [iD],[3] **Sreekanth Manavalla** [iD],[4] **Joshua Stephen Chellakumar Isaac JoshuaRamesh Lalvani** [iD],[5] **P. L. Somasundaram** [iD],[6] **P. Tamilarasu** [iD],[7] **and Prakash Singh Tanwar** [iD][8]

^{1}*Department of Mechanical Engineering, Velammal Engineering College, Chennai, Tamil Nadu, India*
^{2}*Faculty of Mechanical and Production Engineering, Arba Minch Institute of Technology, Arba Minch University, Arba Minch, Ethiopia*
^{3}*Department of Mechanical Engineering, Alagappa Chettiar Government College of Engineering and Technology, Karaikudi, Tamilnadu, India*
^{4}*School of Mechanical Engineering & Electric Vehicles Incubation, Testing and Research Centre, Vellore Institute of Technology Chennai, Vellore, Tamilnadu, India*
^{5}*Faculty of Mechanical and Production Engineering, Arba Minch Institute of Technology, Arba Minch University, Arba Minch, Ethiopia*
^{6}*Department of Electrical and Electronics Engineering, M.Kumarasamy College of Engineering, Karur, Tamil Nadu, India*
^{7}*Department of Electrical and Electronics Engineering, Kongu Engineering College, Perundurai, Tamil Nadu, India*
^{8}*Department of Computer Science and Engineering, Lovely Professional University, Phagwara, Punjab, India*

Correspondence should be addressed to Madhan Mohankumar; madhanesecme08@gmail.com and Joshua Stephen Chellakumar Isaac JoshuaRamesh Lalvani; isaac.jrl@amu.edu.et

Al$_2$O$_3$ with 10 wt.% of SiC ceramic composite is synthesized at 1500°C by electrical resistance heating sintering with a holding time of 5 hours and microwave sintering methods with a holding time of 15 minutes. The samples generated by the two methods are characterized using powder X-ray diffraction and field emission scanning electron microscopy (FESEM). Experiments with both samples showed that the existence of the α-Al$_2$O$_3$ and β-SiC phases in both samples was verified by the findings of XRD pattern on both samples. Microstructure study illustrates that the Al$_2$O$_3$ matrix particles have spherical-like shape and their average matrix particle size is 67 ± 5 nm for electrical resistance heating sintered sample and 38 ± 5 nm for microwave sintered sample. The lattice strain and crystallite size of Al$_2$O$_3$ matrix were measured using Williamson–Hall (W-H) methods, which were achieved via the use of XRD peak broadening, based on a diffraction pattern. Three modified W-H models were used to compute other parameters, including strain (ε) and stress (σ), as well as energy density (u). These models were the uniform deformation model (UDM), the uniform deformation energy density model (UDEDM), and the uniform deformation stress model (UDSM). The average crystallite sizes of α-Al$_2$O$_3$ attained from these three models of Williamson–Hall (W–H) methods and FESEM analysis are correlated and found very close to each other. In all three models of the W-H technique, X-ray diffraction peak profile examination of electrical resistance heating-sintered and microwave-sintered Al$_2$O$_3$/10 wt. % SiC ceramic composite reveals that the microwave-sintered sample has finer crystallite size with less strain.

1. Introduction

Among all the ceramics, alumina (Al_2O_3) are extensively used in engineering applications owing to its thermal and chemical inertness, comparably high strength, and electrical and thermal insulators together with the availability and bounteousness [1–8]. In spite of the abovementioned advantages, brittleness and low fracture toughness of Al_2O_3 create restrictions of its applications. One of the methods to overcome this limitation is the synthesis of fibre or particulate reinforced Al_2O_3 ceramic composites. In this, reinforcement can be a polymer, metal, or ceramics. A ceramic material, silicon carbide (SiC), perchance, is one of the options for the secondary phase which bring about the enhancement of Al_2O_3 matrix [9–14]. Nihara stated that inclusion of SiC particles in little amount to the Al_2O_3 matrix can enhance the mechanical properties of Al_2O_3/SiC structural ceramic composite substantially in comparison with monolithic Al_2O_3 [15–19]. They found that the addition of 5 wt.% SiC as a secondary phase improved the strength and fracture toughness of the material from 350 to 1520 MPa and 3.5 to 4.8 MPam1/2, respectively, by increasing the amount of SiC in the material [15]. There are various ways to sinter this structural ceramic composite such as standard pressureless sintering, hot isostatic pressing, spark plasma sintering, and microwave sintering. Among these, microwave sintering is one of the effective and energy-saving methods which also enhances the mechanical and microstructure of Al_2O_3/SiC ceramic composites [16, 17].

Crystallite size and morphology play vital parts in several applications of the ceramic composites, which have induced the researchers to concentrate on the fabrication methods, type of composites, and sintering methods. XRD peaks' profile investigation has become a very compelling tool for microstructural characterization of ceramics either in bulk or in powder form. It was widely accepted that the Debye–Scherrer technique and the Williamson–Hall method were both appropriate for calculating the lattice strain (ε) and the crystallite size (D) from the broadening of XRD peaks, respectively [18–24]. No material has a perfect crystal structure because of their finite size which leads to an anomaly from ideal crystallinity which produces the X-ray diffraction peak broadening [24, 25]. The information from the pattern obtained from diffractometer apparently gives about the expansion of X-ray diffraction peaks and can be directly quantified. However, it is essential to become aware of that broadening of diffraction peaks arises primarily as a result of the following two factors, namely, crystallite size and lattice strain [26]. It is a common practice to use peak profile analysis of diffraction pattern to estimate microstructural characteristics such as lattice strain and crystallite size, and the findings are compared with the observable attributes of the material [27]. Both the microstructural quantities mentioned above influence the intensity and width of the Bragg peak and produce a 2θ peak position shift.

$Al_2O_3/10$ wt.% SiC ceramic composite is developed in this study using both electrical resistance heating sintering and microwave sintering techniques. To estimate the following microstructural properties, the authors perform an XRD peak profile analysis utilising the Debye–Scherrer and modified Williamson–Hall (W-H) techniques. There are three properties of α-Al_2O_3 that have been determined: crystallite size (D), lattice stress (σ), and lattice stiffness (S). In order to compute the above properties, modified W-H plots were utilised. According to the literature review, a thorough and comparative study of X-ray diffraction peak profile analysis using these modified W–H models on electrical resistance heating sintered and microwave sintered $Al_2O_3/10$ wt.% SiC ceramic composite has not been published.

2. Experimental Procedure

The ceramic composite $Al_2O_3/10$ wt.% SiC was synthesized at 1500°C using electrical resistance heating sintering and microwave sintering techniques. The appropriate weight percentage of Al_2O_3 (Sigma Aldrich Chemicals Pvt Ltd, 99.5%) and SiC (Sigma Aldrich Chemicals Pvt Ltd, 99%) was milled at a speed of 350 rpm for 6 hours with isopropyl alcohol in a planetary ball mill (VB Ceramics, Chennai, India) using tungsten carbide (WC) lined vial and tungsten carbide (WC) ball. After milling, the homogeneous mixture was dried and sieved. With a dwell period of 30 seconds and a pressure of 60 MPa, the homogeneous mixture was compacted into pellets of circular cross section with 5 mm radius and 3 mm thickness using a cold uniaxial press. An initial batch of pellets was sintered at 1500°C for 5 hours in an electrical resistance heating furnace with molybdenum disilicide ($MoSi_2$) as the heating element, and an additional batch of pellets was sintered at the same temperature with a minimum holding time of 15 minutes in a microwave furnace equipped with a magnetron that produces microwaves at 2.45 GHz and a susceptor that served as the axillary heating element. In both the sintering methods, 10°C per minute heating was used. In both the electrical resistance heating furnace and the microwave furnace, the specimens were furnace cooled after they had been sintering. X-ray diffractogram of the synthesized specimens were reported using XRD-Smart Lab (9 kW), Japan, diffractometer with CuKα radiation ($\lambda = 1.54060$ Å) utilising 45 kV and 30 mA as operating conditions. 4° per minute, 0.02° per step, and a scan range of 10° to 90° were the scan speeds, steps angles, and scan ranges, respectively. An FESEM (Supra 55-Carl Zeiss, Germany) was used to examine the morphology of the powders in the sintered sample and estimate their composition. Using ImageJ software, the particle size was calculated using the line interpolation technique.

3. Results and Discussion

3.1. X-Ray Diffraction Analysis. Figure 1 exemplifies the diffractogram of microwave-sintered and electrical resistance heating-sintered $Al_2O_3/10$ wt.% SiC ceramic composite sample, recorded between 10° and 90° of Bragg angle (2θ). All the observed peaks of X-ray diffraction pattern can be indexed with the rhombohedral system of α-Al_2O_3 and β-SiC, referenced in the JCPD's file no. 71–1123 with space group R3c and 89–4793 with space group R3m, respectively.
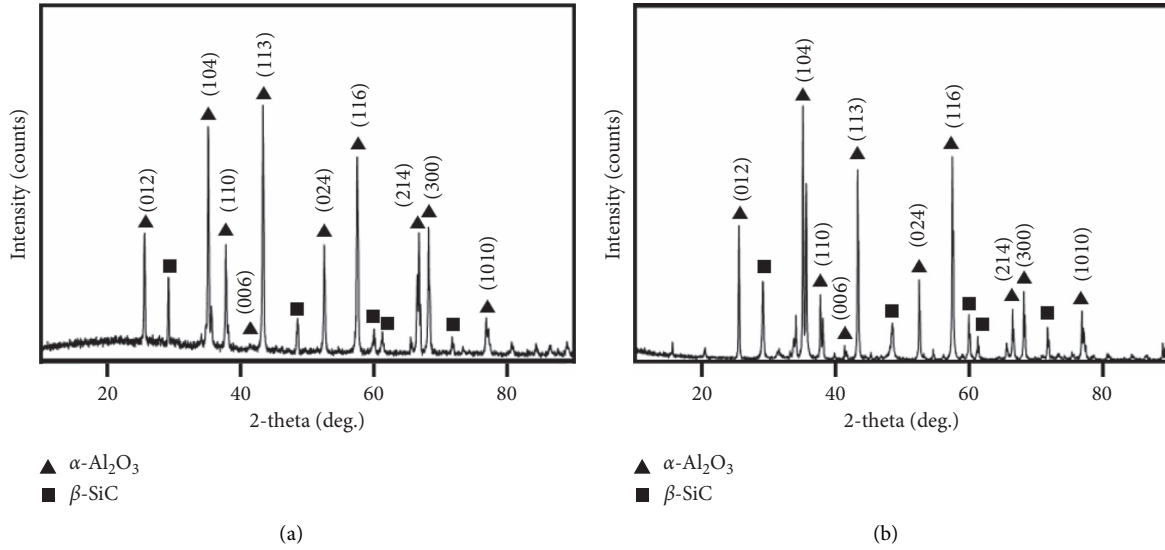
FIGURE 1: XRD pattern of Al_2O_3/10 wt.% SiC: (a) microwave sintered and (b) electrical resistance heating sintered.

The R3c space group has both hexagonal and rhombohedral unit cells. The fundamental structure is made up of hexagonal oxygen planes interspersed with aluminium planes. The R3m space group of β-SiC indicates the rhombohedral polymorphs, which have zigzag atomic position of Si and C.

The lattice parameter of α-Al_2O_3 matrix phase determined from the X-ray diffraction pattern of electrical resistance heating sintered sample were $a = b = 4.758$ Å and $c = 12.998$ Å and microwave sintered samples were $a = b = 4.759$ Å and $c = 12.995$ Å and those relatively close when equated with the lattice parameter of α-Al_2O_3 unit cell were $a = b = 4.761$ Å and $c = 12.99$ Å from the JCPD's file no. 71–1123. In both microwave-sintered and electrical resistance heating-sintered sample, strong and sharp peaks of stable α-Al_2O_3 phase were present and indicate that the samples have crystalline phase, and no other phases of Al_2O_3 were found because the starting powder used was stable α-Al_2O_3. In the X-ray diffraction analysis, it was found that the microwave-sintered sample peaks were more intense than those of the electrical resistance heating-sintered sample, indicating that the microwave-sintered sample exhibits higher levels of crystallinity than the electrical resistance heating sample.

3.2. Crystallite Size and Strain Determination

3.2.1. Debye–Scherrer Method.

In general, the increase in peak width in the X-ray diffractogram and in the peak profile analysis as a result of dislocation growth is by reason of an increase in lattice strain, crystallite size, and instrumental magnification as a result of dislocation growth [28]. The peak broadening caused by instrumental magnification must be taken into consideration while conducting a systematic examination for lattice strain and crystallite size effects. The X-ray diffractogram of a standard Al_2O_3 was obtained in order to isolate the instrumental peak widening from the sample. The corrected peak broadening corresponding to the various peaks of α-Al_2O_3 was calculated using the following equation [29]:

$$\beta_{hkl} = \left[\left(\beta_{hkl} \right)^2_{measured} - \left(\beta_{hkl} \right)^2_{instrumental} \right]^{1/2}. \tag{1}$$

Equation (2) shows how to determine the size of a crystallite using the Scherrer formula, which is given below:

$$D = \frac{k\lambda}{\beta_{hkl} \cos \theta} \Rightarrow \beta_{hkl} = \frac{k\lambda}{D \cos \theta}, \tag{2}$$

where k is the shape factor (0.9), D is the crystallite size in nm, λ is the wavelength of X-ray (Cu Kα = 0.15406 nm), and β_{hkl} is the full width at half maxima (FWHM) of an individual peak at 2θ. Table 1 shows the α-Al_2O_3 average crystallite size of electrical resistance heating-sintered and microwave-sintered Al_2O_3/10 wt.% SiC composite.

3.2.2. Williamson–Hall Method

(1) Uniform Deformation Model (UDM). In addition to the strain, the crystallite size and defects in the crystallite lattice may cause X-ray diffraction peaks to be generated in a variety of other situations. By examining the full width half maximum of the peak as a function of Bragg's angle (2θ), Williamson–Hall analysis clearly separates the peak deformation caused by the crystallite size and the lattice strain [30]. Equation (3) was used to calculate the amount of crystal defect and distortion that produces strain in the powders which results in peak broadening:

$$\varepsilon = \frac{\beta_{hkl}}{4 \tan \theta}. \tag{3}$$

It has been shown that the crystallite size-induced peak width changes as $1/\cos \theta$ and that the lattice strain varies as $\tan \theta$ using equations (2) and (3), respectively. The total peak widening, which is the sum of the peak broadening caused by both lattice strain and crystallite size, is given by [31]

TABLE 1: Results of Debye–Scherrer, WH plots and SEM image

| Method | Debye–Scherer | UDM | | UDSM | | | UDEDM | | | SEM |
	D in nm	D in nm	Strain	D in nm	Strain	Stress σ in MPa	D in nm	Strain	Stress σ in MPa	u in kJm^{-3}	D in nm
Electrical resistance heating sintering	67.15	61.41	4.1E-0.5	70.67	4.3E-0.5	389.81	74.95	4.5E-0.5	394.65	183.34	67 ± 5
Microwave sintering	37.71	37.05	4.7E-0.6	39.63	4.6E-0.6	388.77	40.36	4.6E-0.6	392.43	189.67	38 ± 5

$$\beta_{hkl} = \beta_D + \beta_\varepsilon, \tag{4}$$

where β_D is the peak broadening on account of crystallite size, β_ε is the peak broadening as a result of lattice strain, and β_{hkl} is the instrumental adjusted full width half-maximum intensity of the peak broadening. The value of the instrumentally adjusted full width half-maximum intensity of each peak is calculated using equation (1). Given the assumption of self-reliant contributions of lattice strain and crystallite size to peak broadening, the broadening of the peak is equal to the sum of equations (2) and (3), which is denoted by [32]

$$\beta_{hkl} = \frac{k\lambda}{D \cos \theta} + 4\varepsilon \tan \theta. \tag{5}$$

We may get by rearranging equation (5) the following:

$$\beta_{hkl} \cos \theta = \frac{k\lambda}{D} + 4\varepsilon \sin \theta. \tag{6}$$

Based on the assumption that strain is even in all crystallographic directions, as shown in equation (6), the Williamson–Hall equation, also known as the uniform deformation model (UDM), may be used to predict crystallographic direction in a variety of situations. UDM models assume that crystal nature is isotropic, with the assumption that the material's characteristics are not affected by the direction of measurement in the crystallographic direction, as the case with conventional models. With $\beta_{hkl} \cos \theta$ on the y-axis and $4\varepsilon \sin \theta$ on the x-axis, a graph was created and a linear fit was performed. The y-intercepts of the graph represent the crystallite size (D) of the matrix and the slope

represents the amount of strain (ε) in the α-Al$_2$O$_3$ matrix. While the UDM plots for electrical resistance heating-sintered sample and microwave-sintered sample are shown in Figures 2(a) and 2(b), respectively, and the average crystallite size and lattice strain are shown in Table 1.

(2) Uniform Stress Deformation Model (USDM). In numerous scenarios, the concepts of homogeneity and isotropies are not met. In order to overcome this and assimilate more practical condition, an approach of anisotropic is implemented. Consequently, anisotropic strain (ε) is used to improve the W-H equation. The stress owing to lattice distortion is assumed to be even across all directions of crystallography in the uniform stress deformation model (USDM), presuming particles have only a small microstrain. In uniform stress deformation model (USDM), stress and strain have linear relationship based on Hook's law:

$$\sigma = \varepsilon Y_{hkl} \Rightarrow \varepsilon = \frac{\sigma}{Y_{hkl}}, \tag{7}$$

where σ is the crystal stress, Y_{hkl} is the modulus of elasticity, and ε is the anisotropic microstrain. The Williamson–Hall technique is modified in the USDM method by replacing equation (7) for equation (6) [32]:

$$\beta_{hkl} \cos \theta = \frac{k\lambda}{D} + \frac{4\sigma \sin \theta}{Y_{hkl}}. \tag{8}$$

Equation (9) gives Young's modulus for hexagonal crystal structures [33]:

$$Y_{hkl} = \frac{\left[h^2 + (h+2k)^2/3 + (al/c)^2\right]^2}{S_{11}\left(h^2 + (h+2k)^2/3\right)^2 + S_{33}(al/c)^4 + (2S_{13} + S_{44})\left(h^2 + (h+2k)^2/3\right)(al/c)^2}, \tag{9}$$

where S_{11}, S_{13}, S_{33}, and S_{44} are the elastic compliances of Al$_2$O$_3$ with values 2.3×10^{-12}, 0.4×10^{-12}, 2.2×10^{-12}, and -6.8×10^{-12} m^{2}N^{-1} respectively; "a" and "c" are lattice parameters [34]. By plotting, $\beta_{hkl} \cos \theta$ along the y-axis and $4 \sin \theta / Y_{hkl}$ along the x-axis, the slope of the linear fit provides the uniform stress (σ) and the y-intercept provides the crystallite size (D). The USDM plots for electrical resistance heating-sintered and microwave-sintered Al$_2$O$_3$/10 wt. % SiC samples are shown in Figures 3(a) and 3(b), respectively, and the values of

uniform deformation stress (σ) and crystallite size (D) are included in Table 1.

(3) Uniform Deformation Energy Density Model (UDEDM). The crystal energy density of the sample was calculated using the UDEDM model. Crystals were formerly thought to follow a homogeneous and isotropic model, according to traditional view. Nevertheless, the assumption of homogeneity and isotropy is false in a large number of cases. Furthermore, when examining the deformation energy
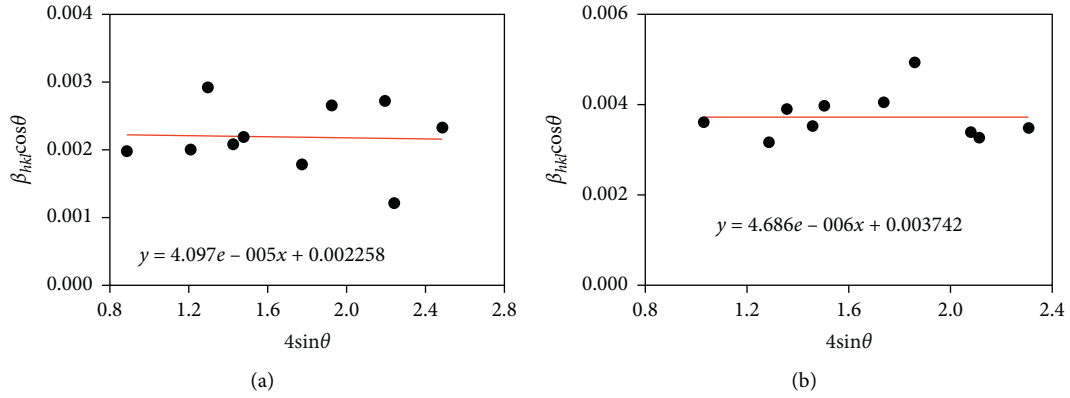
(a)

(b)

FIGURE 2: UDM plot for $Al_2O_3/10$wt. % SiC sample: (a) electrical resistance heating sintering and (b) microwave sintering.
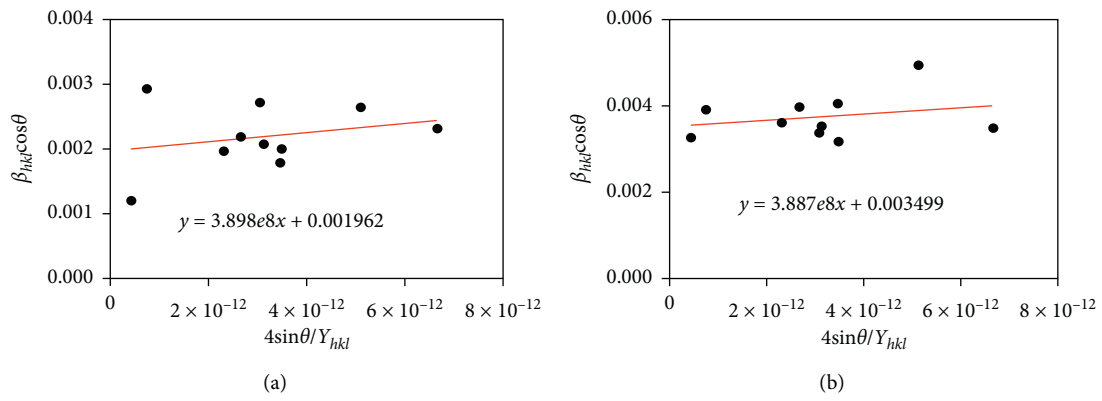

(a)

(b)

FIGURE 3: USDM plot for $Al_2O_3/10$wt. % SiC: (a) electrical resistance heating sintering; (b) microwave sintering.
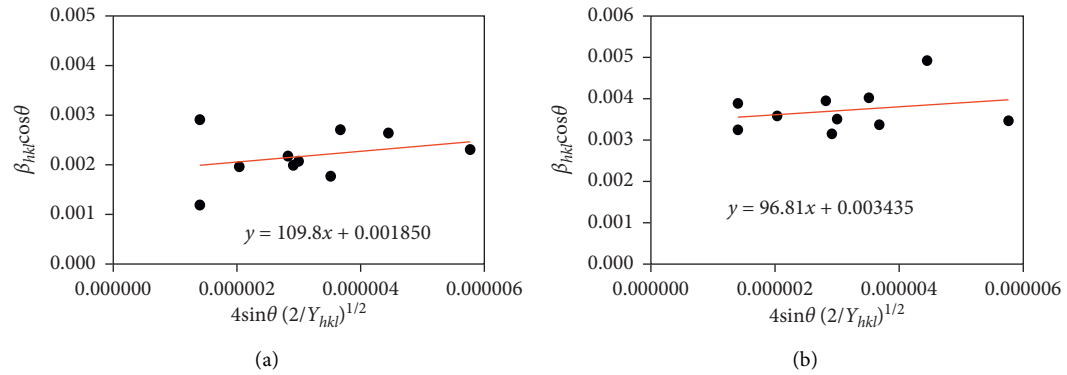

(a)

(b)

FIGURE 4: UDEDM plot for $Al_2O_3/10$wt. % SiC: (a) electrical resistance heating sintering; (b) microwave sintering.

density, the strain-stress connection is not independent. Hooke's law used for an elastic system shows that $u = \varepsilon^2 Y_{hkl}/2$ is used to calculate the density of deformation energy. As a result, equation (9) may be changed as follows based on the energy and strain relationship:

$$\beta_{hkl} \cos \theta = \left(\frac{k\lambda}{D}\right) + \left(4 \sin \theta \left(\frac{2u}{Y_{hkl}}\right)^{1/2}\right). \qquad (10)$$

The UDEDM plots for electrical resistance heating-sintered and microwave-sintered $Al_2O_3/10$ wt. % are shown

in Figures 4(a) and 4(b). The values of anisotropic energy density (u) and average crystallite size (D), which are given in Table 1, are calculated using the slope and Y-intercept.

3.3. Morphological Study.

Figure 5 shows the average matrix particle size and morphology of $Al_2O_3/10$ wt. % SiC-sintered powder as analysed using a field emission scanning electron microscope picture. It can be clearly confirmed that the attained sintered sample powders are spherical in shape with agglomeration of particles. The average matrix particle size
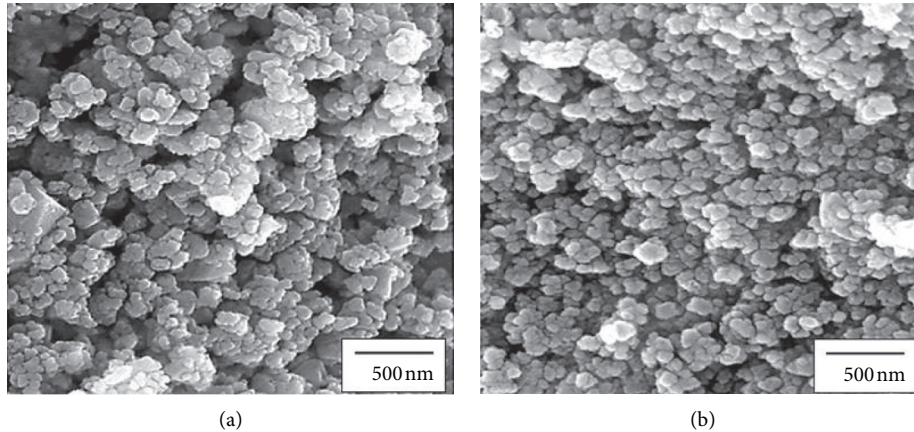
FIGURE 5: SEM image of sintered powder: (a) electrical resistance heating sintered; (b) microwave sintered.

can be seen as 67 ± 5 nm for electrical resistance heating-sintered Al_2O_3/10 wt.% SiC and 38 ± 5 nm for microwave-sintered Al_2O_3/10 wt.% SiC, and the results are very close to the values obtained by Debye–Scherrer and W-H plot. The reason behind the reduction of average matrix particle size of microwave-sintered sample is volumetric heating and less dwell time than electrical resistance heating sintering. The longer dwell time in electrical resistance heating sintering results in grain growth and forms coarse matrix particle, and it was evident in the previous studies [19].

4. Conclusion

Al_2O_3/10 wt. % SiC ceramic composite is successfully synthesized at 1500°C by electrical resistance heating sintering and microwave sintering methods. The electrical resistance heating sintering method has a longer holding time of 5 hours, and microwave sintering has a shorter holding time of 15 minutes. Powder XRD and FESEM are used to characterise the samples from both techniques. The XRD study reveals the existence of α-Al_2O_3 and β-SiC phases in the samples synthesized using both methods, but the intensity of the peaks is higher in the sample synthesized by microwave sintering than in the sample synthesized by electrical resistance heating sintering, indicating that the microwave sintered sample is more densely packed. The lattice parameter of α-Al_2O_3 matrix phase determined from the X-ray diffraction pattern of electrical resistance heating-sintered sample were $a = b = 4.758$ Å and $c = 12.998$ Å and microwave-sintered samples were $a = b = 4.759$ Å and $c = 12.995$ Å. X-ray diffraction peak broadening was evaluated using three models of W-H techniques: the UDM, UDSM, and UDEDM. There was an acceptable degree of accuracy in estimating the values of various physical parameters such as energy density, stress, and strain using these three W-H analysis models; thus, these three W-H plot models are highly sought after for describing crystal perfection. When compared to electrical resistance heating-sintered sample, microwave-sintered sample shows fine crystallite size with less strain. When compared to the W-H techniques, the SEM findings were in close agreement with each other.

Data Availability

The data used to support the findings of this study are included within the article.

Conflicts of Interest

The authors declare that they have no conflicts of interest.

Acknowledgments

References

[1] J. Bai, X. Yang, S. Xu, Y. Shi, and J. Yang, "Fabrication of highly dense Al2O3 ceramics," *Scripta Materialia*, vol. 68, no. 6, pp. 393–395, 2013.

[2] Y.-H. Choa, A. Nakahira, and K. Niihara, "Microstructure and mechanical properties of SiC platelet reinforced Al2O3/SiC-particle hybrid composites," *Journal of Materials Science*, vol. 35, no. 12, pp. 3143–3149, 2000.

[3] Z. B. Yin, C. Z. Huang, B. Zou, H. L. Liu, H. T. Zhu, and J. Wang, "Study of the mechanical properties, strengthening and toughening mechanisms of Al2O3/TiC micro-nano-composite ceramic tool materials," *Materials Science and Engineering A*, vol. 77, pp. 9–15, 2013.

[4] D. Sciti, J. Vicens, and A. Bellosi, "Microstructure and mechanical properties of Alumina-SiC nanocomposite prepared from ultrafine powders," *Journal of Materials Science*, vol. 37, no. 17, pp. 3747–3758, 2002.

[5] Y.-W. Kim and J.-G. Lee, "Pressureless sintering of alumina-titanium carbide composites," *Journal of the American Ceramic Society*, vol. 72, no. 8, pp. 1333–1337, 1989.

[6] S. Yoshioka, L. Boatemaa, S. v. d. Zwaag, W. Nakao, and W. G. Sloof, "On the use of TiC as high-temperature healing particles in alumina based composites," *Journal of the European Ceramic Society*, vol. 36, no. 16, pp. 4155–4162, 2016.

[7] D. Żymełka, S. Saunier, D. Goeuriot, and G. Molimard, "Densification and thermal gradient evolution of alumina during microwave sintering at 2.45 GHz," *Ceramics International*, vol. 39, pp. 3269–3277, 2013.

[8] E. Schafler, M. Zehetbauer, and T. Ungàr, "Measurement of screw and edge dislocation density by means of X-ray Bragg profile analysis," *Materials Science and Engineering*, vol. 319-321, pp. 220–223, 2001.

[9] R. Iglesias, M. A. Rivas, J. C. R. Reis, and T. P. Iglesias, "Permittivity and electric conductivity of aqueous alumina (40nm) nanofluids at different temperatures," *The Journal of Chemical Thermodynamics*, vol. 89, pp. 189–196, 2015.

[10] S. Grasso, T. Saunders, H. Porwal, B. Milsom, A. Tudball, and M. Reece, "Flash spark plasma sintering (FSPS) of α and β SiC," *Journal of the American Ceramic Society*, vol. 99, no. 5, pp. 1534–1543, 2016.

[11] M. Gonon, "Case studies in the X-ray diffraction of ceramics," *Encyclopedia of Materials: Technical Ceramics and Glasses*, vol. 1, pp. 560–577, 2021.

[12] V. Mote, Y. Purushotham, and B. Dole, "Williamson-Hall analysis in estimation of lattice strain in nanometer-sized ZnO particles," *Journal of Theoretical and Applied Physics*, vol. 6, p. 6, 2012.

[13] S. Kalacska, I. Groma, A. Borbely, and P. D. Ispanovity, "Comparison of the dislocation density obtained by HR-EBSD and x-ray profile analysis," *Applied Physics Letters*, vol. 110, Article ID 091912, 2017.

[14] S. Das Bakshi, D. Sinha, and S. Ghosh Chowdhury, "Anisotropic broadening of XRD peaks of α'-Fe: Williamson-Hall and Warren-Averbach analysis using full width at half maximum (FWHM) and integral breadth (IB)," *Materials Characterization*, vol. 142, pp. 144–153, 2018.

[15] C. F. Gutiérrez-GonzálezM. Suarez et al., "Effect of TiC addition on the mechanical behaviour of Al_2O_3–SiC whiskers composites obtained by SPS," *Journal of the European Ceramic Society*, vol. 36, pp. 2149–2152, 2016.

[16] P. Mohanty, S. Mohapatra, J. Mohapatra, S. Singh, P. Padhi, and D. Mishra, "Utilization of chemically synthesized fine powders of SiC/Al_2O_3 composites for sintering," *Materials and Manufacturing Processes*, vol. 31, pp. 1311–1317, 2016.

[17] M. Mohankumar and A. N. Shankar, T. S. Karthick et al., "A comparative study on crack-healing ability of Al_2O_3/SiC structural ceramic composites synthesized by microwave sintering and conventional electrical sintering," *Advances in Materials Science and Engineering*, vol. 2021, p. 8, Article ID 3170697, 2021.

[18] K. Niihara, "New design concept of structural ceramics," *Journal of the Ceramic Society of Japan*, vol. 99, pp. 974–982, 1991.

[19] M. Mohankumar and P. Gopalakrishnan, "Microwave versus conventional sintering: microstructure and mechanical properties of Al_2O_3–SiC ceramic composites," *Boletin de la Sociedad Espanola de Ceramica y Vidrio*, vol. 58, pp. 14–22, 2019.

[20] A. C. Murrieta and F. F. Contreras-Torres, "Microstructure of polycrystalline solids: a brief review from methods in X-ray line profile analysis," *Materials Today: Proceedings*, 2020.

[21] B. Himabindu, N.S.M.P. Latha Devi, and B. R. Kanth, "Microstructural parameters from X-ray peak profile analysis by Williamson-Hall models; A review," *Materials Today: Proceedings*, 2021.

[22] D. Sciti, J. Vicens, and A. Bellosi, "Microstructure and mechanical properties of Alumina-SiC nanocomposite prepared from ultrafine powders," *Journal of Materials Science*, vol. 37, pp. 3747–3758, 2002.

[23] X. L. Shi, F. M. Xu, Z. J. Zhang et al., "Mechanical properties of hot pressed Al_2O_3/SiC composites," *Materials Science and Engineering A*, vol. 527, pp. 4646–4649, 2010.

[24] A. Khorsand Zak, W. H. A.. Majid, and M. E. Abrishami, "Ramin Yousefi, "X-ray analysis of ZnO nanoparticles by Williamson–Hall and size–strain plot methods," *Solid State Sciences*, vol. 13, pp. 251–256, 2011.

[25] S. Mustapha, M. M. Ndamitso1, A. S. Abdulkareem et al., "Comparative study of crystallite size using Williamson-Hall and Debye-Scherrer plots for ZnO nanoparticles," *Advances in Natural Sciences: Nanoscience and Nanotechnology*, vol. 10, Article ID 045013, 2019.

[26] B. Rajesh Kumar and B. Hymavathi, ""X-ray peak profile analysis of solid-state sintered alumina doped zinc oxide ceramics by Williamson–Hall and size-strain plot methods," *Journal of Asian Ceramic Societies*, vol. 5, pp. 94–103, 2017.

[27] B. D. Cullity and S. R. Stock, *Elements of X-ray Diffraction*, Prentice-Hall, Hoboken, NJ, USA, 3rd edition, 2001.

[28] M. Razavi, A. R. Farajipour, M. Zakeri, M. R. Rahimipour, and A. R. Firouzbakht, "Production of Al_2O_3–SiC nano-composites by spark plasma sintering," *Boletin de la Sociedad Espanola de Ceramica y Vidrio*, vol. 56, pp. 186–194, 2017.

[29] K. D. Rogers and P. Daniels, "An X-ray diffraction study of the effects of heat treatment on bone mineral microstructure," *Biomaterials*, vol. 23, pp. 2577–2585, 2002.

[30] C. Suryanarayana and M. G. Norton, *X-ray Diffraction: A Practical Approach*, Plenum Press Publishing, New York, NY, USA, 1998.

[31] V. Biju, N. Sugathan, V. Vrinda, and S. L. Salini, "Estimation of lattice strain in nanocrystalline silver from X-ray diffraction line broadening," *Journal of Materials Science*, vol. 43, pp. 1175–1179, 2008.

[32] T. Pandiyarajan and B. Karthikeyan, "Cr doping induced structural, phonon and excitonic properties of ZnO nanoparticles," *Journal of Nanoparticle Research*, vol. 14, p. 647, 2012.

[33] D. Balzar and H. J. Ledbetter, "Voigt-function modeling in Fourier analysis of size- and strain-broadened X-ray diffraction peaks," *Journal of Applied Crystallography*, vol. 26, pp. 97–103, 1993.

[34] S. Kumar and V. D. Mote, "Ram prakash, vinay kumar, "X-ray analysis of α-Al_2O_3 particles by Williamson–Hall methods," *Materials Focus*, vol. 5, pp. 545–549, 2016.